DOI: 10.1002/adma.201501690
Article type: Communication

Highly Ordered One-Dimensional Fullerene Crystals for Concurrent Control of Macroscopic Cellular Orientation and Differentiation towards Large-Scale Tissue Engineering

Kosuke Minami, Yuki Kasuya, Tomohiko Yamazaki, Qingmin Ji, Waka Nakanishi, Jonathan P. Hill, Hideki Sakai, Katsuhiko Ariga**

Dr. K. Minami, Y. Kasuya, Dr. T. Yamazaki, Dr. Q. Ji, Dr. W. Nakanishi, Dr. J. P. Hill, Prof. Dr. K. Ariga
World Premier International (WPI) Research Center for Materials Nanoarchitectonics (MANA)
National Institute for Material Science (NIMS)
1-1 Namiki, Tsukuba, Ibaraki, 305-0044, Japan
E-mail: K.M. (MINAMI.Kosuke@nims.go.jp)
K.A. (ARIGA.Katsuhiko@nims.go.jp)
Y. Kasuya, Prof. Dr. H. Sakai
Faculty of Science and Technology
Tokyo University of Science
2641 Yamazaki, Noda, Chiba, 278-8510, Japan
Dr. J. P. Hill, Prof. Dr. K. Ariga
Core Research for Evolutional Science and Technology (CREST)
Japan Science and Technology Agency (JST)
Gobancho, Chiyoda-ku, Tokyo 102-0076, Japan

Keywords: tissue engineering, cell scaffold, fullerene, micropatterning

Tissue engineering and regenerative medicine are part of an emerging field involving the development of alternative therapies for tissue- and organ-repair, and remain clinically challenging.[1] Key factors in the field of tissue engineering are the structures and properties of the cell scaffold.[2] The cell scaffold is required to support adhesion, growth and differentiation of cells of the desired phenotype. Cell morphology is also a critical consideration for multicellular tissue formations.[3] Classically, the properties of biomolecules, including growth and transcription factors, have been investigated and have been demonstrated to regulate cell differentiation.[4] Recent studies have also demonstrated that the use of three-dimensional (3D) cell scaffolds in the absence of inductive biomolecules not only provides an appropriate surface but also suitable spaces for cell adhesion, growth and morphological control.[5–8] These 3D structures containing an appropriate surface for cell differentiation are typically required not only to construct a 3D platform but also to functionalize its surface. However, these substrates suffer the disadvantage of complex fabrication processes making the preparation of large-area scaffolds inconvenient.

Since the carbon clusters, including fullerenes, nanotubes and graphenes have become available in large quantities they have attracted significant attention including as potential materials for biological applications, such as drug/gene delivery,[9–12] photodynamic therapy,[12–14] bioimaging [9,12,15] and biosensing,[16] because of their bioavailability and biocompatibility. Because of their unique physicochemical properties, the sp^2-hybridized graphitic structures of carbon clusters have exhibited significant applicability for use as cellular scaffolds in tissue engineering, including for cell adhesion, proliferation and differentiation,[17] especially to promote osteogenic[18] and myogenic differentiation.[19] The π-electronic systems of carbon clusters have been reported to aid in extracellular matrix protein adsorption, which facilitates cell adhesion as well as differentiation by the carbon clusters.[17–20] Although some cellular scaffolds based on carbon nanotubes and graphenes have been used to fabricate large-area scaffolds, they are difficult to construct at the submicrometer-

to micrometer-scale for patterned 3D structures in the absence of a support because of either the nanoscale diameters of 1D carbon nanotubes or the flat structure of 2D graphenes. Moreover, the nanoscale fibrous nature of carbon nanotubes leads to a limitation involving the possibility of inducing mesothelial carcinogenesis due to cell membrane piercing, similarly to asbestos fibers.[21]

Fullerenes are 0-dimensional spherical structures, which exhibit a wide variety of self-assembled structures from 1D to 3D,[22] such as sheets, rods, porous materials and whiskers. Fullerene whiskers (FWs) have been prepared in large scale by using a liquid–liquid interfacial precipitation method,[23] which yields high aspect ratio crystals with submicrometer diameters and lengths in excess of 100 μm. In addition, FWs are biocompatible with macrophages phagocytizing FWs[24] and they exhibit low cytotoxicity.[25] We hypothesized that the micrometer-sized carbon cluster-based material, FWs might be applicable as a cellular scaffold suitable for inducing myogenic differentiation with concurrent control of the growth direction of cells. In particular, the direction of muscle fibers formed during myogenic differentiation might be controlled by the FW orientation (**Figure 1**). The aligned FW was constructed by using the Langmuir-Blodgett (LB) approach.[26] The LB approach is a powerful technique that can be used to assemble large-area monolayers of anisotropic building blocks. Thus, we anticipated that the alignment of FWs as cell scaffolds could affect various aspects of cellular phenotype, including muscle fiber formation, as well as cell adhesion, proliferation and differentiation.

FWs were prepared by the liquid–liquid interfacial precipitation (LLIP) method.[23] For use of FW as a control medium for 1D cell growth, an FW diameter of over 300 nm is required.[5–8] FWs obtained here were 322 ± 108 nm in diameter with lengths of 170 ± 42 μm (aspect ratio = 595) as determined by scanning electron microscopy (SEM) and optical microscopy imaging analysis (Supporting Information, Figure S1). FWs were aligned on a glass substrate by using the LB approach (**Figure 2**a).[26] An isopropanol suspension of FWs was dispersed onto a water surface in a

quartz cell trough (1 cm width × 5 cm length × 4 cm height). At zero or low surface pressure, the FWs assembled into random domains with their long axis parallel to the barrier.[27] The glass plate (1 × 2.5 cm) was inserted at the edge of the FW film, as shown in Figure 2a and was then moved a distance of 3 cm during 30 sec from one side to the other to compress the FW film. The compressed FW film was transferred in a single step onto the bare glass plate by vertically withdrawing the glass substrate again during 30 sec at the tilting angle of the glass substrate θ (Figure 2b). Figure 2c–e show SEM and optical microscopy images of the FW LB film on the glass plate. The FWs were highly aligned on the glass surface with a maximum surface coverage of 79%. The surface coverage could be tuned from 79% at 45° to 59% at 0° by changing the tilt angle θ of the substrate (Figure 2d and e). The highly aligned FW scaffold presents ca. 500 nm ordered groove on the glass surface as determined by atomic force microscopy (AFM) imaging (Figure 2f). The submicrometer-sized grooves are well suited for use for the control of cell orientation.[5–8]

The LB approach can be applied for the alignment of anisotropic building blocks on various substrates without dependence on the nature of the surface, for instance, whether it is hydrophobic or hydrophilic. We also demonstrated the alignment of FWs on surface-modified glass substrates. The substrates were prepared by spin-coating of polymer solutions, poly(sodium 4-styrenesulfonate) (PSS), poly(ethylamine) (PEI) or poly(vinylpyrrolidone) (PVP), or by silanization of the glass using octadecyltriethoxysilane (C18Si), dodecyltrimethoxysilane (C12Si) or [3-(2-aminoethylamino)propyl]triethoxysilane (NH2Si).[28] Although the surface properties of the substrates are different, the alignment and coverage of FWs on the substrates was similar to that on bare glass (Supporting Information, Figure S2). The results indicate that the LB approach of FW can also be applied for alignment of FWs on a wide variety of substrates.

We then investigated the usefulness of the FW-based substrates as cell culture scaffolds, with emphasis on cell adhesion and growth direction. We seeded mouse skeletal myoblast C2C12

cells on an aligned FW-substrate then incubated it for 24 h. We also seeded the cells on randomly aligned FW scaffolds, which had been prepared by simple dropcasting of FWs onto a bare glass plate (see Supporting Information, Figure S1). Cell adhesion on the substrates was analyzed by immunostaining of actin filament and observation of vinculin activity using confocal laser scanning microscopy imaging. The development of actin filament and vinculin activity can be clearly observed coinciding with the edges of FWs (**Figure 3**a). Cells adhered on the bare glass exhibited typical of vinculin patches at their peripheries (Figure 3a, white arrowheads). On the other hand, vinculin-active regions of FWs were distributed uniformly along their lengths, but usual peripheral vinculin patches were not observed. These results indicate that FWs possess surfaces suitable for the adhesion of myoblast cells. We also analyzed morphologies of cells on the different substrates by applying cytoskeleton staining with phalloidin (Figure 3b). Although myoblasts grown on the random FW scaffold had polygonal shapes similar to the cells on the bare glass substrate, the cells on the aligned FW scaffolds exhibited elongated morphologies of high aspect ratios. The elongation of myoblasts was quantified by calculating the aspect ratio of the cells; the cells on bare glass, random FW and aligned FW scaffolds had aspect ratios of 2.26, 2.71 and 4.03, respectively (Figure 3c). Moreover, C2C12 myoblast cells grown on the aligned FW scaffold were well aligned with their growth direction highly correlated with the direction of FW alignment, whereas myoblasts grown on bare glass or the random FW scaffolds, where have no micropatterned architectures of FWs, showed no variations in cell morphology (Figure 3d and e). The shapes of C2C12 cells can be changed by their application to some micropatterned topography.[6] These results suggest that the aligned FW enhanced the elongation of myoblast cells and regulate their growth direction.

According to the morphological analysis, the sizes of cells on the bare glass are larger than those on the FW scaffolds possibly because the cells can spread freely on the glass surface. We also investigated the proliferation and regulation of cell growth direction on the FW-based scaffolds by

analyzing the cell division rate using a fluorometric assay of ATP. The numbers of cells adhered on the FW scaffolds were low relative to that on bare glass at 24 h (Figure 3f). There was a 4-fold increase in the numbers of cells on the aligned FW scaffolds during the subsequent 24 h (24 h to 48 h). This relative increase of cells on the aligned FW scaffolds indicates the low cytotoxicity of FWs. Notably, the growth rate on the aligned FW scaffolds was greater than that on the bare glass, whereas there was no increase in the number of cells on the random FW scaffolds in the same period. These results indicate that the aligned FWs enhanced proliferation of myoblast cells while the randomly deposited FWs suppressed cell growth because the cells surrounded by FWs can not grow across the long-axis of FW (Supporting Information, Figure S3).

It is known that the myogenic differentiation is initiated by the change of cell morphology from triangular to elongated bipolar followed by fusion of mononucleated myoblasts leading to multinucleated myotubes (Figure 3g).[29] Controlling the direction of cell growth and elongation of cell induces the early stage of myogenic differentiation.[6,30] The LB-fabricated aligned FW scaffolds proved submicrometer-scale 1D patterned grooves that are highly likely to promote an elongated morphology in myoblast cells.[7] These results clearly indicate that the aligned FW scaffold strongly influenced the cell growth direction as well as the elongation of cells more effectively than the other so far reported micropatterned scaffold[6] and carbon cluster-based scaffolds,[19] and hence the fullerene-based material, FWs, may induce the early stage of the myogenic differentiation.[30] Moreover, the direction of cell growth and long-axis of elongated myoblast cells are well correlated, which is likely to lead to fusion of the elongated myoblast cells and formation of myotubes.

This micropatterned fullerene-based scaffold may provide a useful platform for the myogenic differentiation. Myotubes or muscle fibers are linear actuators, and hence scaffolds for myogenic differentiation requires *ex vivo* construction of parallel 1D growths of myoblasts as well as myotubes. We further investigated myogenic differentiation including control of the direction of the

myotube formation on the FW-based scaffolds. The C2C12 myoblast cells were incubated in a low serum medium (2% fetal bovine serum (FBS); a differentiation medium) for 10 days, then analyzed for myogenic differentiation and cell growth direction by immunostaining of nuclei and myosin heavy chain (MHC), a protein required for myotube formation.[31] C2C12 myoblasts fused to form multinuclear myotubes, in which the local density of FWs did not influence the formation of multinuclear myotubes (**Figure 4**a and b, and Supporting Information, Figure S4). The fusion index was analyzed by calculating the ratio of multinuclear MHC-positive cells to the total number of nuclei.[6] The fusion index increased from 12.3% on glass to 23.2% on the aligned FW scaffold (Figure 4c), suggesting that the FWs stimulate myoblast fusion. Importantly, the direction of myotube formation was strongly coherent with the direction of the aligned FWs while on bare glass lacking a micropatterned FW support the myoblasts were randomly fused.

Myogenic differentiation requires the upregulation of the myogenic regulatory factor family (MRF) genes, *MyoD* and *Myf5*.[32] Myoblasts were differentiated to myotubes, which express the late MRFs, *Myogenin* and *MRF4*, and subsequently express muscle-specific genes, such as *MHC* and muscle creatine kinase (*MCK*).[31,32] To investigate the expression of myogenic genes, we analyzed the expression of *MyoD* and *Myogenin* by quantitative RT-PCR after differentiation for 10 days (Figure 4d). The expression level of *MyoD* was enhanced 1.35-fold for cells on the aligned FW compared with those on bare glass. *Myogenin* on the aligned FW scaffold was also subject to enhanced expression at 1.43-fold greater than for cells on bare glass. The level of upregulation was comparable to the reported carbon cluster-based scaffolds.[19] This significant upregulation of the myogenic genes indicates that the LB-fabricated 1D patterned FWs not only accelerated both early and late stages of myogenic differentiation but also controlled both the growth and fusion directions leading to the formation of well-oriented myotubes, and hence our aligned FW scaffolds will be suitable for use as a scaffold for regeneration of skeletal muscle tissues, overcoming the structural

limitations faced by other carbon cluster materials, such as carbon nanotubes or graphenes.[17,19]

In conclusion, we have demonstrated that aligned 1D FW scaffolds induce myogenic differentiation from myoblast to myotube. FWs were precisely prepared in submicrometer- to micrometer-scale, which were suitable for controlling cellular morphology.[7] These microsmeter-scale FWs were aligned on substrates by a simple method using the interfacial alignment leading to up to 79% coverage to construct 1D micropatterned architectures without any other patterned supports, regardless of the identity of the base substrate, including those formed from hydrophilic or hydrophobic materials. While both the aligned FW and random FW scaffolds exhibited cell adhesion and proliferation, the 1D-patterned architecture of the aligned FW substrate showed significant enhancement of myogenic differentiation and regulated the direction of myotube formation. This approach for the alignment of micrometer-scale 1D materials used in this study can potentially be applied for the fabrication of large area assemblies of anisotropic materials.[26] With its potential to induce myogenic differentiation, and to control growth direction, as well as its biocompatibility, our aligned FW scaffolds are promising platforms for a useful alternative to micropatterned cell scaffolds for tissue engineering.

Experimental Section

Preparation of aligned FW scaffold: Fullerene whiskers (FWs) were prepared by the liquid–liquid interfacial precipitation method by a reported procedure.[23] Briefly, isopropanol (5 mL) was carefully layered onto a saturated toluene solution of C_{60} (5 mL) in a glass bottle at room temperature, and the solution was kept at 20 °C for 7 days. The resulting FW suspension was centrifuged at 4000 rpm for 2 min, the supernatant was decanted, and the solid washed once with isopropanol. The purified FWs were redispersed and stored in isopropanol (5 mL) at room temperature prior to use. FWs were characterized by optical microscopy (BX-51, OLYMPUS, Japan) and scanning electron microscopy

(S-4800, HITACHI, Japan).

An aligned FW substrate was prepared by a method similar to the Langmuir–Blodgett (LB) approach. A suspension of FW in isopropanol (0.2 mL) was spread gently onto the surface of pure water (18 mL) in a quartz trough (inner cavity of the trough was 1 cm width × 5 cm length × 4 cm height), and incubated for 3 min to form an FW film at the air–water interface. A bare glass plate (1 cm x 2.5 cm), which had been washed with acetone, methanol, and water just prior to use, was inserted at the edge of the trough and compressed to form the aligned FW film during 30 sec. Then the aligned FW film was transferred onto the glass plate by withdrawing it with a tilt angle θ ($0\,^\circ < \theta < 45\,^\circ$) during 30 sec (Figure 2b). The aligned FW scaffold was dried under reduced pressure for 15 h. Randomly deposited FW scaffold was prepared by dropcasting. A suspension of FWs in IPA (0.2 mL) was deposited on a bare glass plate, and was then dried under reduced pressure for 15 h.

Cell line: Mouse skeletal myoblast C2C12 cells (RCB0987) were provided by the Riken Bio Resource Center and maintained in DMEM with 10% FBS, 100 units penicillin, and 100 μg streptomycin (growth medium) at 37 °C in a humidified atmosphere with 5% CO_2.

Cell adhesion and morphology analysis on the FW scaffolds: C2C12 cells were washed 3 times with PBS, lifted by incubation with trypsin at 37 °C for 2−3 min, and resuspended in growth medium. The C2C12 suspension was pipetted onto each substrate placed in a 10 cm plastic dish at a density of 1×10^4 cells/cm^2. After incubation for 24 h, cell growth direction and morphology were analyzed by immunostaining and image analysis.

To evaluate the cell adhesion on the aligned FW scaffolds, vinculin activity and actin filament were analyzed by immunostaining. For staining of vinculin, C2C12 cells were immunostained following a reported procedure.[33] In brief, the cells were fixed with 4%

paraformaldehyde solution in PBS for 15 min. After soaking in PBS containing 0.2% Triton X-100 for 5 min, the cells were blocked with 1% BSA in PBS for 30 min, and subsequently incubated with 1:400 hVIN-1 (ab11194, Abcam, Japan) for 1 h. The cells were stained with a 1:1000 fluorescent labeled goat anti-mouse antibody (Alexa-Fluor 488, A11001, Invitrogen, USA) for 1 h in the dark, with 1:50 Phalloidin (Alexa-Fluor 594, A12381, Invitrogen, USA) for 20 min in the dark, and with 0.1% DAPI for 5 min in the dark. The immunostained cells were imaged using a confocal laser scanning microscopy (CLSM) (TCS-SP5, Leica).

To evaluate the cell morphology, cytoskeleton was analyzed by fluorescent imaging. For staining of cytoskeleton, the cells were fixed with 4% paraformaldehyde for 10 min. After soaking in PBS containing 0.1% Triton X-100 for 5 min, the cells were stained with 1:500 Phalloidin (Alexa-Fluoro 488, A12379, Invitrogen, USA) for 20 min in the dark, and with 0.1% DAPI for 5 min in the dark. The C2C12 cells were imaged with a Fluorescence Microscope (Leica, DM2500). The cell aspect ratio and growth direction were quantified from isolated cells by using ImageJ software. The cell growth direction is defined as the angle of deviation of myoblast from the principal axis of the cell islands. The angle of aligned FW under the cell was measured. Edges and regions without good stamping or cell adhesion were not used for analysis.

Myotube formation analysis on FW scaffolds: For myogenic differentiation, the culture medium was replaced with differentiation medium (DMEM with 2% FBS, 100 units penicillin, and 100 μg streptomycin) after incubation for 24 h. The differentiation medium was replenished every 2 days during the culture period. To evaluate the myotube formation analysis, myosin heavy chain (MHC) was analyzed by immunostaining. To investigate the myogenic gene expression, cell lysate was removed, then scaffolds were transferred into fresh wells. ISOGEN reagent was added into each well, and then the samples were transferred into fresh tubes and stored at –80 °C until use for quantitative

real-time RT-PCR.

For immunostaining of myosin heavy chain, the cells were immunostained following a reported procedure.[34] In brief, the cells were fixed with 4% paraformaldehyde for 12 min. After soaking in PBS containing 0.3% Triton X-100 for 5 min, the cells were blocked with 5% bovine serum albumin (BSA) in PBS for 15 min, and subsequently stained with a 0.1% MY-32 (ab-7784, Abcam, Japan) for 24 h at 4 ºC. The cells were stained with a 0.1% fluorescent labeled goat anti-mouse antibody (AlexaFluor 488, A11001, Invitrogen, USA) for 1 h in the dark, with 0.1% DAPI for 5 min in the dark. The immunostained cells were imaged with a CLSM (TCS-SP5, Leica). The fusion index was calculated as the ratio of the nuclei number in myotubes with two or more nuclei versus the total number of nuclei.[6] Edges and regions that did not show good stamping or cell adhesion were not used for analysis. At least five images on each substrate were used for quantitative analysis.

RNA extraction and quantitative real-time RT-PCR analysis: Total RNA was extracted using ISOGEN reagent (NIPPON GENE). To obtain cDNA of the transcripts, the reverse transcriptase reaction was performed with 0.5 μg of total RNA (PrimeScript RT reagent Kit, TaKaRa). Quantitative real-time RT-PCR was performed with the synthetic cDNA and primer sets for *MyoD* (forward, 5′-CCCAATGCGATTTATCAGGT-3′; reverse, 5′-AGAACGGCTTCGAAAGG-3′);, *Myogenin* (forward, 5’-TGTCTGTCAGGCTGGGTGTG-3’; reverse, 5’-TCGCTGGGCTGGGTGTTAG-3’); and for *GAPDH* as an internal control (forward, 5’-AACTTTGGCATTGTGGAAGG-3’; reverse, 5′-CACATTGGGGGTAGGAACAC-3′) using LightCycler FastStart DNA Master Plus SYBR Green Ⅰ (Roche) in a LightCycler 1.5 (ST300, Roche). The PCR products were analyzed using LightCycler Software ver.3.5 (Roche).

Regulation of cell growth direction by the FWs: Viability of cells at 24 h and 48 h after cell culture on each scaffold was determined by using CellTiter-Glo Luminescent Cell Viability Assay (Promega, USA) following the manufacturer's protocol. After the cell culture on each scaffold for 24 h and 48 h, the scaffolds were transferred into fresh 12-well plates with 250 μL of assay solution. The cells on the scaffolds were dissolved using an orbital plate shaker at 800 rpm for 2 min. After incubation for 10 min, 200 μL of the cell lysates was transferred into a 96-well plate. Fluorescence of the samples was measured using a microplate reader (MTP-880, CORONA).

Statistical analysis: Differences between the experimental groups were detected using Student's t test. Values are expressed as ± SEM; $p < 0.05$ was considered as significant.

Supporting Information

Supporting Information is available from the Wiley Online Library or from the author.

Acknowledgments

This work was partly supported by World Premier International Research Center Initiative (WPI Initiative), MEXT, Japan, the Core Research for Evolutional Science and Technology (CREST) program of Japan Science and Technology Agency (JST), Japan, and Japan Society for the Promotion of Science (JSPS) KAKENHI Grant Number 26104541 and 15K17890. This study was supported by NIMS Molecule & Material Synthesis Platform in "Nanotechnology Platform Project" operated by MEXT, Japan. K.M. thanks YAMATO-MANA program, NIMS.

Competing financial interests

The authors declare no competing financial interests.

Received: ((will be filled in by the editorial staff))
Revised: ((will be filled in by the editorial staff))
Published online: ((will be filled in by the editorial staff))

References

[1] a) A. J. Salgado, J. M. Oliveira, A. Martins, F. G. Teixeira, N. A. Silva, N. M. Neves, N. Sousa, R. L. Reis, *Int. Rev. Neurobiol.* **2013**, *108*, 1; b) D.-H. Park, C. V. Borlongan, D. J. Eve, P. R. Sanberg, *Med. Sci. Monit.* **2008**, *14*, RA206.

[2] a) R. Langer, J. P. Vacanti, *Science* **1993**, *260*, 920; b) A. Atala, F. K. Kasper, A. G. Mikos, *Sci. Transl. Med.* **2012**, *4*, 160rv12; c) S. Pina, J. M. Oliveira, R. L. Reis, *Adv. Mater.* **2015**, *27*, 1143.

[3] M. P. Lutolf, J. A. Hubbell, *Nat. Biotechnol.* **2005**, *23*, 47.

[4] a) M. Schuldiner, O. Yanuka, J. Itskovitz-Eldor, D. A. Melton, N. Benvenisty, *Proc. Natl. Acad. Sci. USA* **2000**, *97* 11307; b) A. Gupta, D. T. Leong, H. F. Bai, S. B. Singh, T.-C. Lim, D. W. Hutmacher, *Biochem. Biophys. Res. Commun.* **2007**, *362*, 17; c) D. T. Leong, W. M. Khorm F. T. Chew, T.-C. Lim, D. W. Hutmacher, *Cells Tissues Organs* **2006**, *182*, 1; d) D. T. Leong, M. C. Abraham, S. N. Rath, T.-C. Lim, F. T. Chew, D. W. Hutmacher, *Differentiation* **2006**, *74*, 519; e) D. T. W. Leong, D. W. Hutmacher, F. T. Chew, T.-C. Lim, *J. Dermatol. Sci.* **2005**, *37* 169.

[5] a) C. Y. Tay, S. A. Irvine, F. Y. C. Boey, L. P. Tan, S. Venkatraman, *Small*, **2011**, *7*, 1361; b) C. Y. Tay, C. G. Koh, N. S. Tan, D. T. Leong, L. P. Tan, *Nanomedicine* **2013**, *8*, 623

[6] a) P. Bajaj, B. Reddy Jr., L. Millet, C. Wei, P. Zorlutuna, G. Bao, R. Bashir, *Integr. Biol.* **2011**, *3*, 897; b) P. Y. Wang, H. T. Yu, W. B. Tsai, *Biotechnol. Bioeng.* **2010**, *106*, 285.

[7] C. J. Bettinger, R. Langer, J. T. Borenstien, *Angew. Chem. Int. Ed.* **2009**, *48*, 5406.

[8] a) T. Yu, C. K. Chua, C. Y. Tay, F. Wen, H. Yu, J. K. Y. Chan, M. S. K. Chong, D. T. Leong, L. P. Tan, *Macromol. Biosci.* **2013**, *13*, 799; b) H. Li, F. Wen, Y. S. Wong, F. Y. C. Boey, C. S. Subbu, D. T. Leong, K. W. Ng, G. K. L. Ng, L. P. Tan, *Acta Biomater.* **2012**, *8*, 531; c) C. Y. Tay, M. Pal, H. Yu, W. S. Leong, N. S. Tan, K. W. Ng, S. Venkatraman, F. Boey, D. T. Leong, L. P. Tan, *Small* **2011**, *7*, 1416; d) C. Y. Tay, H. Yu, M. Pal, W. S. Leong, N. S. Tan, K. W. Ng, D. T. Leong, L. P. Tan, *Exp. Cell*

Res. **2010**, *316*, 1159.

[9] R. Partha, J. L. Conyers, *Int. J. Nanomedicine* **2009**, *4*, 61.

[10] K. Minami, K. Okamoto, K. Harano, K. Doi, E. Noiri, E. Nakamura, *Sci. Rep.* **2014**, *4*, 4916.

[11] B. S. Wong, S. L. Yoong, A. Jagusiak, T. Panczyk, H. K. Ho, W. H. Ang, G. *Adv. Drug Deliv. Rev.* **2013**, *65*, 1964.

[12] K. Yang, L. Feng, X. Shi, Z. Liu, *Chem. Soc. Rev.* **2013**, *42*, 530.

[13] R. Singh, S. V. Torti, *Adv. Drug Deliv. Rev.* **2013**, *65*, 2045.

[14] S. A. Chechetka, B. Pichon, M. Zhang, M. Yudasaka, S. Bégin-Colin, A. Bianco, E. Miyako, *Chem.–Asian J.* **2015**, *10*, 160.

[15] K. Kostarelos, A. Bianco, M. Prato, *Nat. Nanotech.* **2009**, *4*, 627.

[16] Y. Liu, X. Dong, P. Chen, *Chem. Soc. Rev.* **2012**, *41*, 2283–307.

[17] a) W. Nakanishi, K. Minami, L. K. Shrestha, Q. Ji, J. P. Hill, K. Ariga, *Nano Today* **2014**, *9*, 378; b) B. S. Harrison, A. Atala, *Biomaterials* **2007**, *28*, 344.

[18] a) S. Ryu, C. Lee, J. Park, J. S. Lee, S. Kang, Y. D. Seo, J. Jang, B.-S. Kim, *Angew. Chem. Int. Ed.* **2014**, *53*, 9213; b) T. R. Nayak, H. Andersen, V. S. Makam, C. Khaw, S. Bae, X. Xu, P.-L. R. Ee, J.-H. Ahn, B. H. Hong, G. Pastorin, B. Özyilmaz, *ACS Nano* **2011**, *5*, 4670.

[19] S. H. Ku, C. B. Park, *Biomaterials* **2013**, *34*, 2017.

[20] S. Namgung, T. Kim, K. Y. Baik, M. Lee, J.-M. Nam, S. Hong, *Small* **2011**, *7*, 56.

[21] H. Nagai, S. Toyokuni, *Cancer Sci.* **2012**, *103*, 1378.

[22] a) L. K. Shrestha, Q. Ji, T. Mori, K. Miyazawa, Y. Yamauchi, J. P. Hill, K. Ariga, *Chem.–Asian J.* **2013**, *8*, 1662; b) L. K. Shrestha, Y. Yamauchi, J. P. Hill, K. Miyazawa, K. Ariga, *J. Am. Chem. Soc.* **2013**, *135*, 586.

[23] K. Miyazawa, Y. Kuwasaki, A. Obayashi, M. Kuwabara, *J. Mater. Res.* **2002**, *17*, 83.

[24] S. Nudejima, K. Miyazawa, J. Okuda-Shimazaki, A. Taniguchi, in *Advances in biomedical research, proceedings, recent advances in biology and biomedicine,* (Eds: P. Anninos, M. Rossi, T. D.

Pham, A. Bussing, M. Koukkou), WSEAS Press, **2010**, pp 89–94.

[25] J. Okuda-Shimazaki, S. Nudejima, S. Takaku, K. Kanehira, S. Sonezaki, A. Taniguchi, *Health* **2010**, *2*, 1456.

[26] a) I. Patla, S. Acharya, L. Zeiri, J. Israelachvili, S. Efrima, Y. Golan, *Nano Lett.* **2007**, *7*, 1459; b) A. Tao, F. Kim, C. Hess, J. Goldberger, R. He, Y. Sun, Y. Xia, P. Yang, *Nano Lett.* **2003**, *3*, 1229.

[27] S. Acharya, A. B. Panda, N. Belman, S. Efrima, Y. Golan, *Adv. Mater.* **2006**, *18*, 210.

[28] M. Qin, S. Hou, L. Wang, X. Feng, R. Wang, Y. Yang, C. Wang, L. Yu, B. Shao, M. Qiao, *Colloid. Surf. B Biointerfaces* **2007**, *60*, 243.

[29] a) C. R. Caper, *J. Biophys. Biochem. Cytol.* **1960**, *7*, 559; b) A. J. Wagers, L. M. Conboy, *Cell* **2005**, *122*, 659.

[30] N. T. Swailes, M. Colegrave, P. J. Knight, M. Peckham, *J. Cell Sci.* **2006**, *119*, 3561.

[31] M. J. Wakelam, *Biochem. J.* **1985**, *228*, 1.

[32] S. B. P. Chargé, M. A. Rudnicki, *Physiol. Rev.* **2004**, *84*, 209.

[33] T. Naganuma, E. Traversa, *Biomaterials* **2014**, *35*, 4441.

[34] S. Ahadian, J. Ramón-Azcón, M. Estili, X. Liang, S. Ostrovidov, H. Shiku, M. Ramalingam, K. Nakajima, Y. Sakka, H. Bae, T. Matsue, A. Khademhosseini, *Sci. Rep.* **2014**, *4*, 4271.

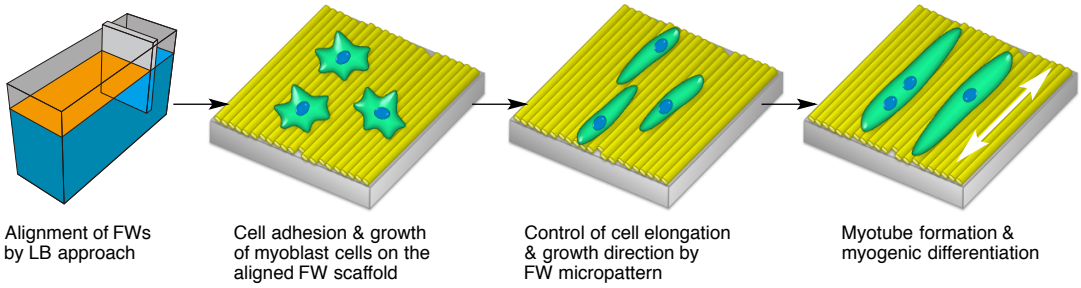

Figure 1. Schematic illustration of myogenic differentiation on highly aligned FW scaffolds. A dispersion of FWs was spread on an air–water interface to form FW film then the FW film was compressed using a glass plate to align FWs into a 2D assembly. Myoblasts on the aligned FW scaffold grow and elongate their shape according to the micropattern of FW. The elongated myoblasts fuse to form multinuclear myotubes during the myogenic differentiation process.

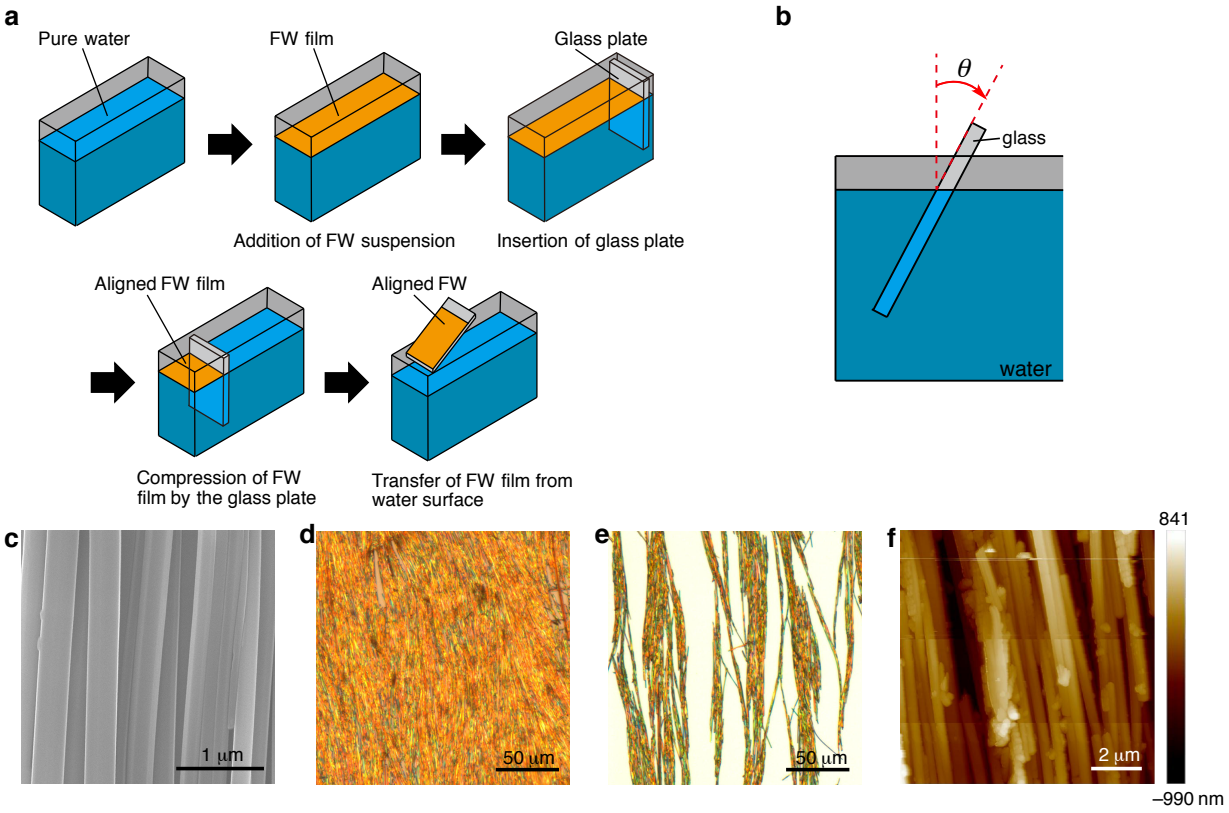

Figure 2. Preparation of aligned FW scaffold. **a**, A schematic illustration of the preparation of aligned FW scaffold by the Langmuir-Blodgett approach. An IPA suspension of FWs was spread carefully on a pure water surface. After formation of the FW film, a glass plate was inserted into one edge of the FW film, and the FW film was compressed using the glass plate to form an aligned FW film. The compressed FW film was transferred onto the glass plate. **b**, A schematic illustration of the tilting angle of the glass plate θ(°). **c**–**f**, Microscopic images of the aligned FW scaffolds taken by SEM (**c**), optical microscopy (**d**) and AFM (**f**) at the withdrawing angle of 45 °, and optical microscopy image of low coverage aligned FW scaffolds at the withdrawing angle of 90 ° (**e**).

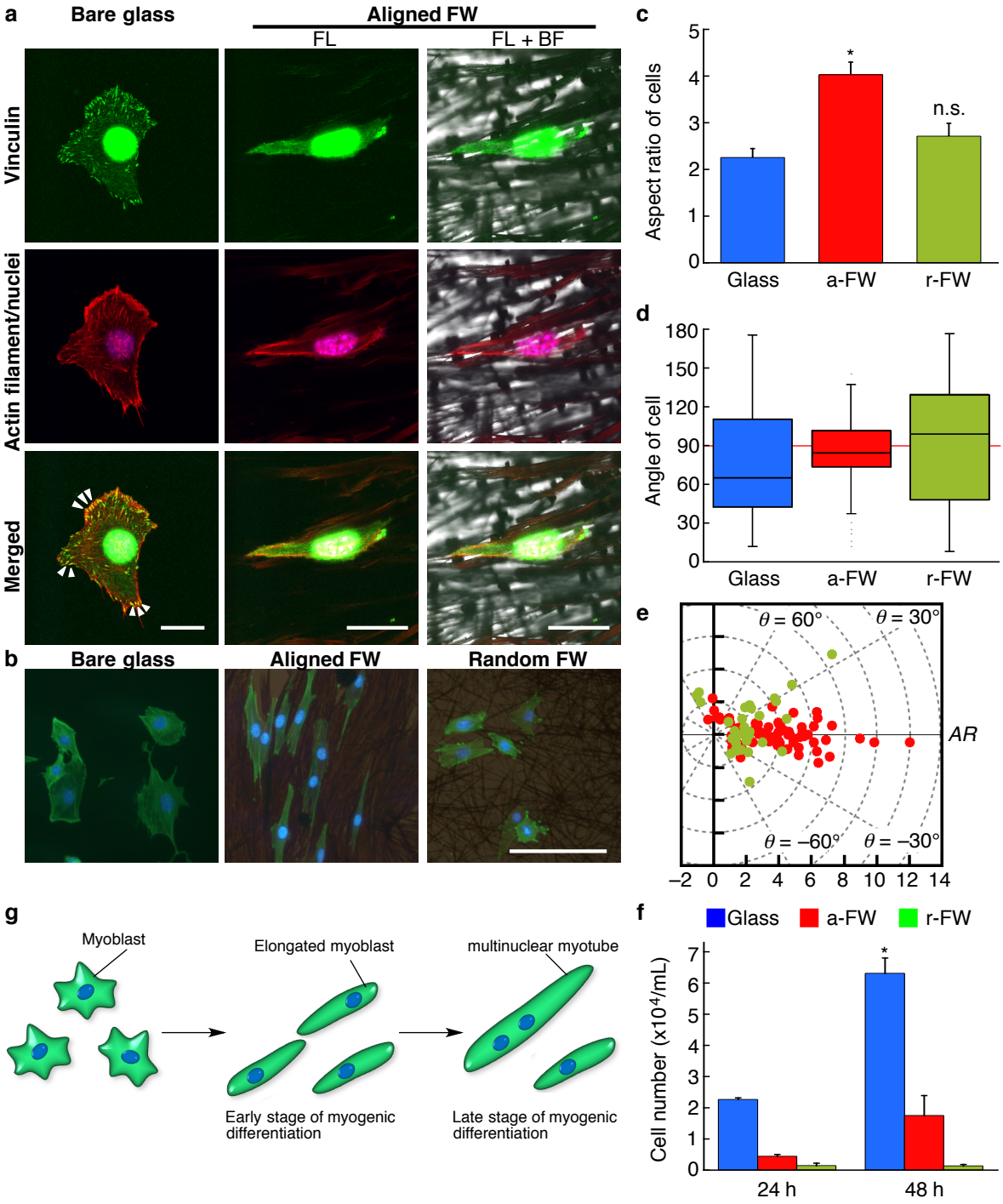

Figure 3. Cell adhesion and growth direction of C2C12 myoblast cells on the aligned FW scaffold. **a**, Immunostaining of vinculin (green) and actin-filament (red) of C2C12 myoblast cells cultured on bare glass and on the aligned FW scaffolds for 24 h. The white arrowheads indicate the vinculin peripheral patches. The colocalized region of vinculin and actin-filament placed along the edge of FW. Scale bars are 25 μm. **b**, Fluorescent staining of cytoskeleton (green) and nucleus (blue) of C2C12 myoblast cells cultured on the bare glass (left), and the aligned (center) and random FW scaffolds (right) for 24 h. Scale bar is 200 μm. **c**, Aspect ratio of C2C12 myoblast cells cultured on bare glass (blue), and aligned (red) and random FW scaffolds (green) for 24 h. **d**, Growth direction of C2C12 myoblast cells on bare glass and FW scaffolds. Box plot of the growth direction of the cells.

θ(°) is the angle subtended by the long axis of the cell and the *x*-axis defined as the long axis of the glass slide. a-FW and r-FW indicate the aligned FW and random FW scaffolds, respectively. All error bars show the SEM. * $P < 0.05$. **e**, Polar plot of the elongation and orientation of cells on the aligned FW scaffolds (red) and on the random FW scaffolds (green). In the polar plot, *AR* is the aspect ratio of the cell, and the angle of difference from FW alignment, θ(°), is the angle between the long axis of the cell and the FW directly under the nucleus. **f**, Fluorometric ATP assay of C2C12 myoblast cells cultured on the scaffolds for 24 and 48 h. Blue, red and green bars indicate the relative cell proliferation on the bare glass, aligned and random FW scaffolds, respectively. All error bars show ±SEM. a-FW and r-FW indicate the aligned FW and random FW scaffolds, respectively. All error bars show the SEM. * $P < 0.05$. **g**, Schematic illustration of myogenic differentiation. Polygonal myoblasts cells grow elongated cells at the early stage of myogenesis, and then fuse to form a myotube.

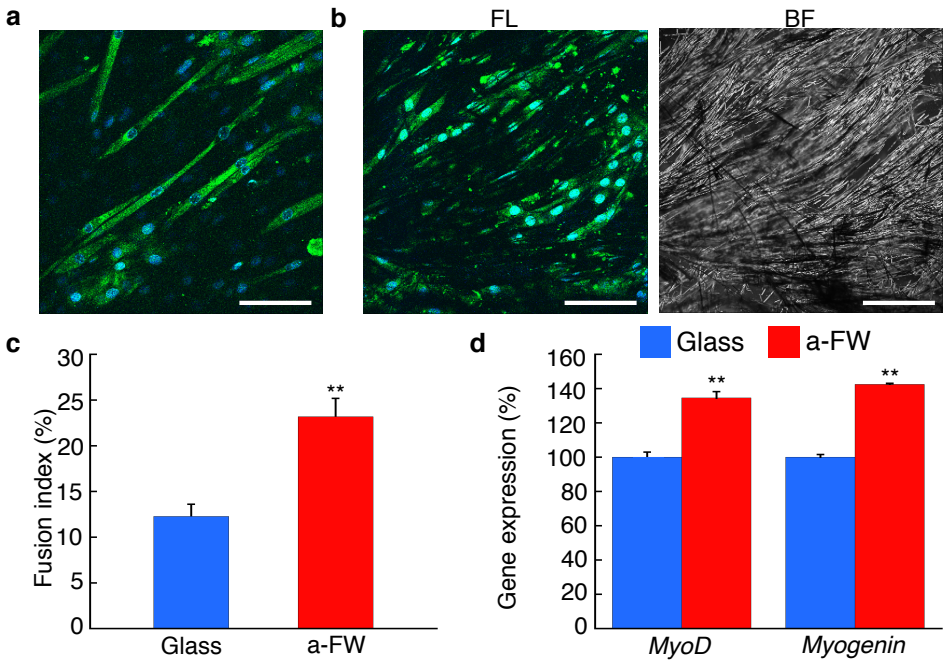

Figure 4. Myogenic differentiation of C2C12 cells with control of the direction of myotube formation on the aligned FW scaffold. **a**,**b**, Immunostaining of the fast skeletal myosin heavy chain (green) and nucleus (blue) of C2C12 cells cultured on bare glass (**a**) and on the aligned FW (a-FW) scaffolds with bright field (BF) image (**b**) and for 10 days in the differentiation media. Scale bars are 100 μm. **c**, Fusion index of the C2C12 cells on each scaffold ($N = 5$ with over 150 cells for each high power field). **d**, The expression level of *MyoD* and *myogenin* was detected by a quantitative real-time RT-PCR analysis ($N = 3$ for each group). All error bars show ±SEM. ** $P < 0.005$ *versus* bare glass.